

# Surfing the shape resonances at the $\text{LaAlO}_3/\text{SrTiO}_3$ interface

D. Valentinis, S. Gariglio, A. Fête, J.-M. Triscone, C. Berthod, and D. van der Marel

Department of Quantum Matter Physics (DQMP), University of Geneva,  
24 quai Ernest-Ansermet, 1211 Geneva 4, Switzerland

(Dated: November 23, 2016)

Superconductivity develops in bulk doped  $\text{SrTiO}_3$  and at the  $\text{LaAlO}_3/\text{SrTiO}_3$  interface with a dome-shaped density dependence of the critical temperature  $T_c$ , despite different dimensionalities and geometries. We propose that the  $T_c$  dome of  $\text{LaAlO}_3/\text{SrTiO}_3$  is a shape resonance due to quantum confinement of superconducting bulk  $\text{SrTiO}_3$ . We substantiate this interpretation by comparing the exact solutions of a two-band BCS gap equation in 3D and quasi-2D. Such comparison highlights the role of heavy bands for  $T_c$  in both geometries. For bulk  $\text{SrTiO}_3$ , we extract the density dependence of the pairing interaction by fit to experimental data. We apply quantum confinement in a square potential well of finite depth and calculate  $T_c$  in the confined configuration. We compare the calculated  $T_c$  to transport experiments and provide an explanation as to why the optimal  $T_c$ 's are so close to each other in 2D interfaces and the 3D bulk material.

Ten years after the discovery of superconductivity at the interface between  $\text{LaAlO}_3$  and  $\text{SrTiO}_3$  (LAO/STO) [1], a consensus on the mechanism has not surfaced. This problem stands out with particular importance, at a crossroads between the fundamental understanding of transition-metal oxides and the engineering of new electronic properties at oxide interfaces. The key question is whether the source of pairing in the two-dimensional electron liquid (2DEL) is the same as in bulk STO, or whether it is an emergent property of the interface. A variety of arguments support each scenario. STO exhibits superconductivity when doped with niobium, lanthanum, or oxygen vacancies [2, 3]. It is the first oxide superconductor ever discovered, and furthermore presents a dome-shaped  $T_c$  versus doping relation reminiscent of the high- $T_c$  copper oxides. The 2DEL also presents a dome-shaped superconducting region when carrier density is tuned by field effect [4–6], with the same maximum  $T_c$  as STO. As it turns out, however, the domes in STO and LAO/STO exhibit many differences, even though the height of their maxima is similar. On the other hand, the reduced dimensionality of the 2DEL invites to consider unconventional superconductivity. The confinement of the carriers, within a thickness of typically 10 nm at low temperature, is revealed by several measurements including transport [1, 4], atomic-force microscopy [7], infrared ellipsometry [8], and confirmed by electronic structure calculations [9]. Consequently, 2D fluctuations have been invoked to explain differences between the bulk and interface superconductivities [4, 10]. Singlet-triplet mixing due to Rashba coupling in the interface electric field may also take place [11, 12], as well as doping-dependent changes in the band structure due to differentiated Hartree shifts in the 3d shell [13]. Another scenario refers to disorder-induced phase separation and percolation [14].

In a broad perspective, the LAO/STO 2DEL may be regarded as an instance of quasi-2D superconductor produced by the confinement of a three-dimensional superconductor in a film geometry [15]. The quantum confinement is a well known strategy for changing  $T_c$ , which has been continuously explored theoretically and experimentally from the

sixties [16, 17]. The vertical localization of electronic states in the film changes the pairing strength, and the formation of subbands leads to oscillations of  $T_c$ —often termed shape resonances—as a function of confinement length and/or carrier density. In this context, the different  $T_c$  behaviors in STO and LAO/STO do not rule out a common mechanism. On the contrary, the quantum confinement *causes* the interface to behave differently than the bulk.

In this Letter, we propose an interpretation of the dome in LAO/STO as the result of a shape resonance triggered by the confinement of carriers at the STO surface. We support this scenario by a microscopic calculation which reproduces both STO and LAO/STO superconducting domes using the same pairing model, taking into account confinement effects for the latter. We also report new measurements of the 2DEL thickness, which allow us to directly compare both systems in spite of their different dimension. According to the new interpretation, the differences between the two domes confirm the commonality of the pairing mechanism for the 2D and 3D cases. LAO/STO offers new opportunities to study shape resonances, thanks to a continuously tunable carrier density, in contrast to metallic thin films whose thickness can only be changed discontinuously in increments of one unit cell. Our modeling furthermore clarifies the roles of the STO light and heavy bands in the LAO/STO superconductivity, showing that  $T_c$  is controlled almost exclusively by the heavy one.

The approach we follow is first to build a minimal model able to capture the density dependence of  $T_c$  in bulk STO with a small number of parameters. We then confine this model along one dimension, set the carrier density to the equivalent 3D density for the 2DEL, and obtain a prediction for  $T_c$  in the confined geometry. The conversion from the measured 2D density of the 2DEL to a 3D density uses the measured 2DEL superconducting thickness. We will first describe the model we use for bulk STO, next describe recent experimental data by some of us on the 2DEL thickness [18], and then present the theoretical results for the 2DEL dome.

Focusing on the essential ingredients, we opt for two parabolic bands and a BCS pairing interaction to describe

STO. The low-energy sector of the STO conduction band involves three bands with mostly Ti 3d character, split by crystal field and spin-orbit interaction [19, 20]. We discard one band lying 30 meV above the other two and not occupied at the densities considered in this study. The bare masses of the remaining two bands and their splitting at the  $\Gamma$  point are chosen such that the 2D density of states evaluated at  $k_z = 0$  with the tight-binding and parabolic dispersions agree at best. We then renormalize both band masses by a factor two representing the effect of electron-phonon coupling and the emergence of large polarons [21, 22]. The resulting band structure is shown in Fig. 1(a), where the parameters are indicated as well. The pairing mechanism in STO is still debated [23, 24]. Standard phonon-mediated pairing is questioned because the low density of STO puts it in the anti-adiabatic regime  $E_F < \hbar\omega_D$ , where  $E_F$  and  $\hbar\omega_D$  are the Fermi and Debye energies, respectively. Leaving alone the origin of pairing, it is believed that STO is amenable to a BCS description with low coupling constants of the order of 0.1–0.3 [19, 20]. We adopt a local BCS interaction of strength  $V$  with a dynamical cutoff  $\hbar\omega_D = 44$  meV, consistent with the Debye temperature of STO [25]. The interaction is the same in both bands and we neglect inter-band coupling for simplicity. In this model, for  $V$  independent of density  $n$ , the critical temperature can only increase with increasing  $n$  [26, 27], in contradiction with the observations [2, 3]. To explain the dome,  $V$  must drop with increasing  $n$  [3]. We fix the  $n$ -dependent interaction such that the model reproduces the  $T_c(n)$  data of Ref. 3. This dataset is preferred because it covers a broad range of densities, but this choice does not affect any of our conclusions. The resulting interaction decreases monotonically with increasing  $n$  as shown in the inset of Fig. 1(b). We interpolate this dependency to get a continuous parametrization  $V(n)$ . The main panel of Fig. 1(b) displays the data of Ref. 3 on top of the continuous  $T_c(n)$  curve resulting from that interpolation. The calculation takes full account of the energy-dependent DOS, including the fact that  $E_F < \hbar\omega_D$ , and uses the self-consistent chemical potential calculated at  $T_c$  [27]. With this parametrization the heavy band starts to be populated before the first maximum of the double dome, as shown by quantum oscillations [3]. A glimpse at the band structure and the value of  $\hbar\omega_D$  reveals that the heavy band contributes to the pairing instability even when it is not populated (see arrows in Fig. 1) [28].

Our hypothesis is that the pairing strength at the LAO/STO interface follows the bulk interaction  $V(n)$ . The carrier density varies across the 2DEL following the profile of the confinement potential, such that the pairing strength would be, strictly speaking, a function of position. As the coherence length is large (50–100 nm) compared with the typical confinement length ( $\approx 10$  nm), which itself is only marginally larger than the Fermi wavelength [7], we use an average  $V$  associated with the average carrier density  $n = n_{2D}/L$ . The density integrated along the confinement direction,  $n_{2D} = \int_{-\infty}^{\infty} dz n(z)$ , has been determined by mea-

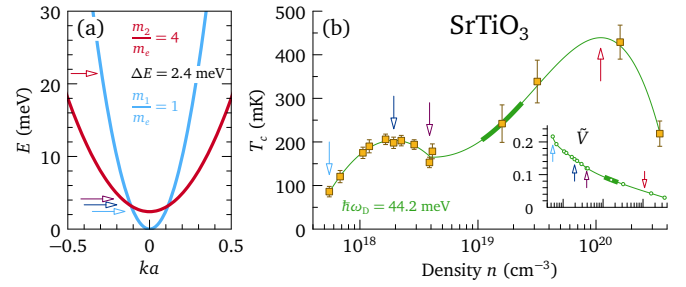


FIG. 1. Weak-coupling model for the density-dependent superconductivity of SrTiO<sub>3</sub>. (a) Parabolic approximation for the bottom of the conduction band;  $\Delta E$  is the band splitting at  $k = 0$ . (b) Data of Ref. 3 (squares with error bars) and calculated  $T_c(n)$  curve (solid line). (Inset) Dimensionless interaction strength [27]  $\tilde{V} = 2V[m_e/(2\pi\hbar^2)]^{3/2}\sqrt{\hbar\omega_D}$  reproducing the experimental  $T_c$  (circles) and interpolation (solid line). The colored arrows indicate remarkable values of  $T_c$  in (b) and the corresponding values of the chemical potential in (a). The thick lines in (b) mark the range of densities visited at the LAO/STO interface.

suring the Hall sheet conductance [4]. For an estimation of the effective 2DEL thickness  $L$  [18], we resort to the analysis of the superconducting transitions measured in magnetic fields [29], applied perpendicular and parallel to the interface [30].

Figure 2 displays the thicknesses and critical temperatures measured as a function of the Hall density  $n_{2D}$  [18]. The dependence  $T_c(n_{2D})$  draws a dome with maximum at 365 mK. The measured thickness is close to 10 nm except at densities above  $2.5 \times 10^{13} \text{ cm}^{-2}$  where it increases steadily. Fig. 1(b) shows that the field-effect doping at the interface explores a relatively narrow density range (thick line) compared with the chemical doping.

Knowing the equivalent 3D density  $n = n_{2D}/L$  for each measured  $n_{2D}$ , we can determine the pairing strength  $V(n)$  in the 2DEL. We model the confinement by taking the band structure of Fig. 1(a) into a square potential well of width  $L$  and depth  $U$ , following Ref. 17. This leads to the formation of 2D subbands at energies that depend on  $L$  and  $U$ . All subbands are coupled by the pairing interaction, which furthermore gets renormalized by the confinement and becomes a function of the band and subband indices via the bound wave functions. The potential well at the LAO/STO interface is certainly not square, but its precise shape is unknown. The formation of 2D bands, interpreted as confinement-induced subbands, is observed experimentally [9, 31, 32], but their occupations and energies are uncertain, preventing us from reconstructing a more realistic potential. We do not expect qualitative changes in our conclusions on going from a square to a triangular or self-consistent confinement potential. The square well moreover has the advantage that the pairing matrix elements are known analytically [17]. The only unknown parameter of our model is therefore  $U$ , whose order of magnitude is estimated from first-principles calculations to be a few

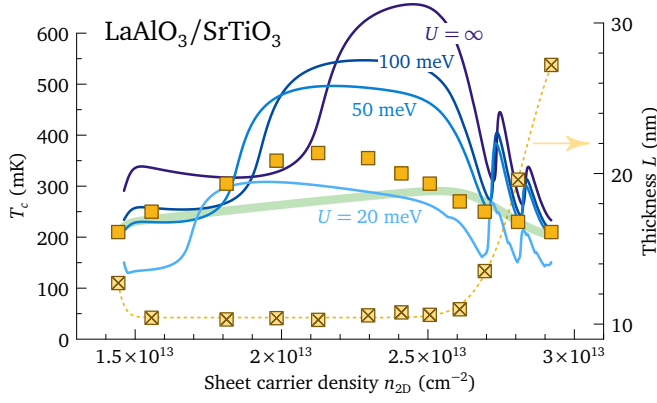


FIG. 2. 2DEL critical temperature (squares) and thickness (crossed squares, right scale) measured at the LAO/STO interface as a function of sheet carrier density. The solid lines show the calculated  $T_c$  obtained by confining the model of Fig. 1 in a square potential well of width  $L$  and various depths  $U$  as indicated. A continuous interpolation of the thickness as a function of density (dotted) was used. For each couple  $(n_{2D}, L)$ , the pairing interaction is read from the inset of Fig. 1(b) at the density  $n = n_{2D}/L$ . The thick line shows the 3D  $T_c$  at density  $n$ .

tens of meV [33]. Figure 2 compares  $T_c$  calculated in the square well for various  $U$  with the measured  $T_c$  of the 2DEL. The calculation yields critical temperatures similar to those measured and a dome-shaped density dependence for all  $U$ . This is our main result: localizing STO carriers at a density  $\sim 10^{19} \text{ cm}^{-3}$  into a  $\sim 10 \text{ nm}$  thick layer leads, owing to quantum confinement effects, to a dome in  $T_c$  as a function of sheet carrier density between  $1.5$  and  $3 \times 10^{13} \text{ cm}^{-2}$ , with a maximum similar to the maximum  $T_c$  of bulk STO. As  $L$  becomes large, for  $n_{2D} > 2.5 \times 10^{13} \text{ cm}^{-2}$ , the calculated  $T_c$  approaches the 3D value (green line) with rapid oscillations for all  $U$ . The measured  $T_c$  is also very close to the 3D value in this regime, where  $T_c$  drops because  $n$  actually decreases with increasing  $n_{2D}$ . In the range where  $L \approx 10 \text{ nm}$ , the 3D  $T_c$  raises monotonically like in Fig. 1, and one notices a density-dependent critical  $U$ , above which the  $T_c$  at the interface is higher than in the bulk [17].

In order to better understand the nature of the dome and disclose more explicitly the connection with shape resonances, we now refine our model to achieve semi-quantitative agreement with the experiment. First, remembering that we mimic a quasi-triangular well by a square one, and also because a systematic error in the experimental determination of  $L$  cannot be excluded, we replace the measured 2DEL thickness  $L_{\text{exp}}$  by  $L = \alpha L_{\text{exp}}$  when comparing model and experiment. Second, an increase of the splitting  $\Delta E$  is expected at the interface, since both strain and electric field contribute directly to the 4-fold crystal field. A modified screening also modifies the Hartree shifts of the bands [13]. We adopt the simple dependence  $\Delta E = \Delta E_{\text{STO}}(1 + \lambda/L)$  with the fit parameter  $\lambda$ , which ensures that the bulk STO splitting is recovered for a thick well. Finally, the confinement potential  $U$  is in principle linked with  $n_{2D}$  and  $L$  via

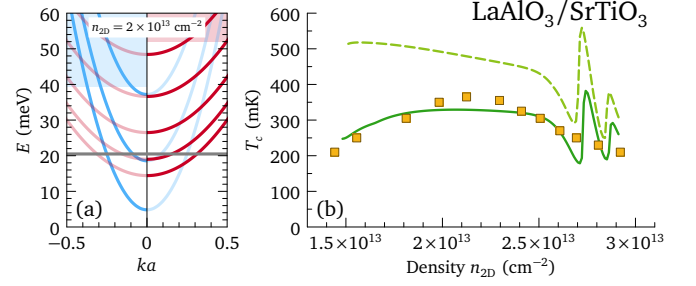


FIG. 3. (a) Subband structure in a quantum well of width  $6.8 \text{ nm}$  and depth  $39 \text{ meV}$  for a band splitting  $\Delta E = 12.9 \text{ meV}$ , corresponding to  $n_{2D} = 2 \times 10^{13} \text{ cm}^{-2}$ . The bound light (heavy) subbands with energies below  $U$  ( $U + \Delta E$ ) are shown on the left (right). The chemical potential  $\mu = 20.5 \text{ meV}$  is also indicated. (b) Measured critical temperature (squares) and calculated  $T_c$  (solid line) for a band splitting  $\Delta E_{\text{STO}}(1 + \lambda/\alpha L_{\text{exp}})$  and a potential  $U = e^2 n_{2D} \alpha L_{\text{exp}} / (\epsilon_0 \epsilon)$  with  $\alpha = 0.65$ ,  $\lambda = 30 \text{ nm}$ , and  $\epsilon = 630$ . The dashed line shows  $T_c$  calculated with the same  $\alpha$ ,  $\lambda = 12 \text{ nm}$ , and  $\epsilon = 377$ .

Poisson's equation. The simplest relation results from dimensional analysis as  $U = e^2 n_{2D} L / (\epsilon_0 \epsilon)$ . The model parameters are adjusted to get the best fit displayed in Fig. 3(b), with  $\alpha = 0.65$ ,  $\lambda = 30 \text{ nm}$ , and  $\epsilon = 630$ . The result  $\alpha < 1$  is expected, because a square well of width  $L_{\text{exp}}$  hosts an electron gas thicker than a triangular well of the same width. Moreover the effective thickness  $\alpha L_{\text{exp}} \approx 7 \text{ nm}$  matches the value measured by AFM [34]. Figure 3(a) shows the subband structure with a splitting five times larger than the bulk splitting at a density  $2 \times 10^{13} \text{ cm}^{-2}$ . We find that two light and two heavy subbands are partly occupied. Photoemission measurements have reported two light subbands lying below the lowest heavy band [35]; our model reproduces this configuration at densities larger than  $2.8 \times 10^{13} \text{ cm}^{-2}$ . The Hall-coefficient nonlinearity observed in Ref. 5 at  $1.6 \times 10^{13} \text{ cm}^{-2}$  corresponds in our model to entering the second heavy subband. Finally, the fitted dielectric constant is consistent with the high polarizability of STO: it agrees well with the value  $\epsilon = 600$  obtained from the low-temperature field-dependent dielectric function of STO, given approximately by  $\epsilon = 1 + \chi_0 / (1 + \mathcal{E}/\mathcal{E}_0)$  with  $\chi_0 = 24000$  and  $\mathcal{E}_0 = 110 \text{ kV/m}$  [7, 36], if we substitute for  $\mathcal{E}$  the order of magnitude of the interface electric field, e.g.,  $\mathcal{E} = U/(eL) = 4.3 \text{ mV/nm}$  at  $n_{2D} = 1.5 \times 10^{13} \text{ cm}^{-2}$ .

Although we have until now compared the critical temperature with the mean-field  $T_c$  from the calculation, in Fig. 3(b) we show that the model is not inconsistent with the pseudogap scenario suggested by tunneling experiments [37], in which the mean-field  $T_c$  continues to increase as the density is reduced, while the critical temperature is suppressed by 2D fluctuations.

In a thin-film geometry, the critical temperature of a weak-coupling BCS superconductor is a continuous oscillating function of the film thickness  $L$  and electron density  $n$  [17]. Pronounced oscillations due to the rapid change in  $L$  are visible in Figs. 2 and 3(b), but not resolved in the experiment.



Note that the detailed oscillating behavior is very sensitive to the approximations made for the shape of the potential well. Using our square-well model, we plot in Fig. 4 the evolution of  $T_c$  as a function of both  $L$  and  $n_{2D} = nL$  in the domain of thicknesses and densities relevant for the 2DEL. The experimental data are shown for comparison at the rescaled thickness  $\alpha L_{\text{exp}}$ . The  $T_c$  landscape in the  $(L, n_{2D})$  plane is rich and displays three types of structures. To describe the features we start at 5 nm thickness, and follow the doping from zero upwards. At the lowest doping  $T_c$  is exponentially small and reaches a first low- $T_c$  step near  $8 \times 10^{12} \text{ cm}^{-2}$ , before raising steeply to  $\sim 400 \text{ mK}$  for doping of the order of  $10^{13} \text{ cm}^{-2}$ . At this thickness and for the doping range displayed in the figure, superconductivity is entirely in the two heavy subbands (the two lowest red curves in Fig. 3). The low- $T_c$  stage corresponds to the first heavy subband, with a  $T_c$  suppressed by a shallow confinement potential (see Fig. 2 for the effect of  $U$  on  $T_c$ ) [17]. For fixed 2D carrier density, the number of occupied subbands varies with the layer thickness as  $(n_{2D}L^2)^{1/3}$ . Since  $T_c$  passes through a maximum when a new heavy subband becomes occupied, the effect of increasing the thickness results in a succession of  $T_c$  maxima; the amplitude of these oscillations decays rapidly with increasing thickness since the layer becomes more and more like a 3D bulk sample with carrier density approaching zero according to  $n = n_{2D}/L$ . The location of maxima is given approximately by  $n_{2D} \approx \frac{\pi}{12}p(p+1)(4p+5)/L^2$  with integer  $p$ . The scars running at a small angle with respect to the first maximum are slope changes of  $T_c$  occurring when a new heavy subband gets bound in the well as  $L$  increases, leading to a slight  $T_c$  enhancement. The very faint lines almost parallel to the density axis indicate that a new heavy subband enters the pairing window at  $\mu + \hbar\omega_D$ . These features reflect that in our calculation we use a BCS-type model interaction with a sharp cutoff at  $\hbar\omega_D$ . Finally,  $\mu$  crossing the third light subband gives another faint structure crossing the previous ones and ending at zero density near  $L = 20 \text{ nm}$ ; other structures associated with the light band are too weak to be visible. Moving up in density for  $L = 20 \text{ nm}$ ,  $T_c$  becomes distinguishable from zero for  $n_{2D} = 3.6 \times 10^{12} \text{ cm}^{-2}$ , and rises in a succession of steps, each corresponding to a new heavy subband becoming occupied. In the limit of infinite thickness the 3D situation depicted in Fig. 1 is ultimately obtained, but since  $n_{2D} = nL$  the superconducting dome shifts out of the 2D doping range displayed in this figure. The figure illustrates that many combinations of thickness and doping parameters can result in a dome-like doping or thickness dependence of  $T_c$ , however the maximal value of  $T_c$  itself is never strongly different from  $T_c^{\text{max}}$  observed in optimally doped bulk STO. We believe that this theoretical observation provides the main clue as to why  $T_c$  is so similar in bulk and interface superconductivity: The pairing potential is basically the same in all cases. Tuning of the density of states by 2D confinement allows the effective pairing interaction to be varied to a certain extent, but its main effect is to define the subband structure. Optimal  $T_c$  is found for

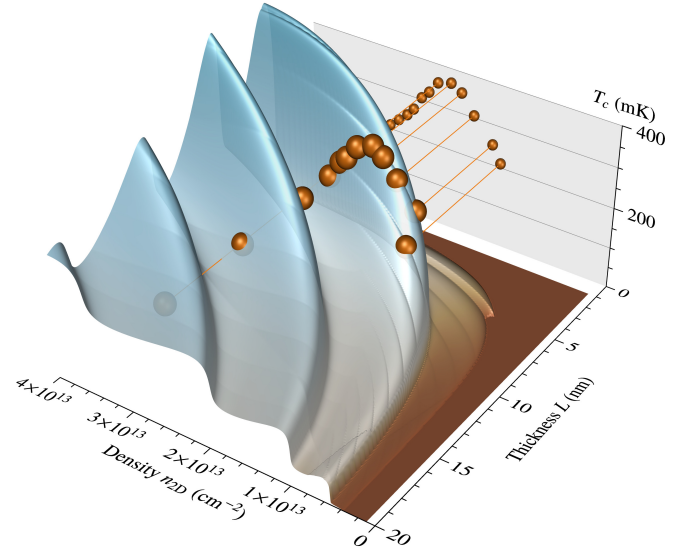


FIG. 4. Critical temperature as a function of thickness  $L$  and sheet carrier density  $n_{2D}$ . The spheres show the experimental data of Fig. 2 where the thickness has been reduced by a factor  $\alpha = 0.65$ . The shaded surface shows the  $T_c$  calculated with a band splitting  $\Delta E_{\text{STO}}(1 + \lambda/L)$  in a square well of width  $L$  and depth  $U = e^2 n_{2D} L / (\epsilon_0 \epsilon)$ , with  $\lambda = 30 \text{ nm}$ , and  $\epsilon = 630$ .

small densities, which holds true in bulk 3D and quasi-2D alike, thus leading to very similar values of the optimal  $T_c$  in 2D and 3D systems.

In summary, we have explored the hypothesis that the pairing potential responsible for superconductivity is the same in 2D interfaces and 3D bulk  $\text{SrTiO}_3$ . We showed that the superconducting dome in the 2D material corresponds to a much narrower effective doping range than in the 3D material, and the optimal  $T_c$  in this case coincides with a shape resonance due to the onset of occupation of one of the subbands created by the 3D confining potential. We have shown that the optimal  $T_c$  should be very similar in the 2D and 3D cases. Potential for optimization of  $T_c$  is offered by tuning the confinement potential  $U$ , which in principle allows  $T_c$  to be increased up to a factor 3, and by controlled tuning of the thickness parameter  $L$  on the 1 nm scale.

This work was supported by the Swiss National Science Foundation through grants n° 200021-153405 and 200021-162628.

- 
- [1] N. Reyren, S. Thiel, A. D. Caviglia, L. F. Kourkoutis, G. Hammerl, C. Richter, C. W. Schneider, T. Kopp, A.-S. Rüetschi, D. Jaccard, M. Gabay, D. A. Müller, J.-M. Triscone, and J. Mannhart, *Science* **317**, 1196 (2007).
  - [2] J. F. Schooley, W. R. Hosler, and M. L. Cohen, *Phys. Rev. Lett.* **12**, 474 (1964); J. Schooley, W. Hosler, E. Ambler, J. Becker, M. Cohen, and C. Koonce, *Phys. Rev. Lett.* **14**, 305 (1965);

- C. S. Koonce, M. L. Cohen, J. F. Schooley, W. R. Hosler, and E. R. Pfeiffer, *Phys. Rev.* **163**, 380 (1967).
- [3] X. Lin, G. Bridoux, A. Gourgout, G. Seyfarth, S. Krämer, M. Nardone, B. Fauqué, and K. Behnia, *Phys. Rev. Lett.* **112**, 207002 (2014).
- [4] A. D. Caviglia, S. Gariglio, N. Reyren, D. Jaccard, T. Schneider, M. Gabay, S. Thiel, G. Hammerl, J. Mannhart, and J.-M. Triscone, *Nature* **456**, 624 (2008).
- [5] A. Joshua, S. Pecker, J. Ruhman, E. Altman, and S. Ilani, *Nat. Comm.* **3**, 1129 (2012).
- [6] C. Bell, S. Harashima, Y. Kozuka, M. Kim, B. G. Kim, Y. Hikita, and H. Y. Hwang, *Phys. Rev. Lett.* **103**, 226802 (2009); J. A. Bert, K. C. Nowack, B. Kalisky, H. Noad, J. R. Kirtley, C. Bell, H. K. Sato, M. Hosoda, Y. Hikita, H. Y. Hwang, and K. A. Moler, *Phys. Rev. B* **86**, 060503 (2012).
- [7] O. Copie, V. Garcia, C. Bödefeld, C. Carrétéro, M. Bibes, G. Herranz, E. Jacquet, J.-L. Maurice, B. Vinter, S. Fusil, K. Bouzehouane, H. Jaffrès, and A. Barthélémy, *Phys. Rev. Lett.* **102**, 216804 (2009).
- [8] A. Dubroka, M. Rössle, K. W. Kim, V. K. Malik, L. Schultz, S. Thiel, C. W. Schneider, J. Mannhart, G. Herranz, O. Copie, M. Bibes, A. Barthélémy, and C. Bernhard, *Phys. Rev. Lett.* **104**, 156807 (2010).
- [9] S. Gariglio, A. Fête, and J.-M. Triscone, *J. Phys.: Condens. Mat.* **27**, 283201 (2015).
- [10] L. Benfatto, C. Castellani, and T. Giamarchi, *Phys. Rev. B* **80**, 214506 (2009).
- [11] L. P. Gor'kov and E. I. Rashba, *Phys. Rev. Lett.* **87**, 037004 (2001).
- [12] M. S. Scheurer and J. Schmalian, *Nat. Comm.* **6**, 6005 (2015).
- [13] E. Maniv, M. Ben Shalom, A. Ron, M. Mograbi, A. Palevski, M. Goldstein, and Y. Dagan, *Nat. Comm.* **6**, 8239 (2015).
- [14] S. Caprara, F. Peronaci, and M. Grilli, *Phys. Rev. Lett.* **109**, 196401 (2012); S. Caprara, J. Biscaras, N. Bergeal, D. Bucheli, S. Hurand, C. Feuillet-Palma, A. Rastogi, R. C. Budhani, J. Lesueur, and M. Grilli, *Phys. Rev. B* **88**, 020504 (2013).
- [15] A. Bianconi, D. Innocenti, A. Valletta, and A. Perali, *J. Phys.: Conf. Ser.* **529**, 012007 (2014).
- [16] C. J. Thompson and J. M. Blatt, *Phys. Lett.* **5**, 6 (1963).
- [17] D. Valentini, D. van der Marel, and C. Berthod, *Phys. Rev. B* **94**, 054516 (2016), and references therein.
- [18] S. Gariglio, M. Gabay, and J.-M. Triscone, *APL Mater.* **4**, 060701 (2016).
- [19] D. van der Marel, J. L. M. van Mechelen, and I. I. Mazin, *Phys. Rev. B* **84**, 205111 (2011).
- [20] S. J. Allen, B. Jalan, S. Lee, D. G. Ouellette, G. Khalsa, J. Jaroszynski, S. Stemmer, and A. H. MacDonald, *Phys. Rev. B* **88**, 045114 (2013).
- [21] D. M. Eagles, *Phys. Rev.* **181**, 1278 (1969).
- [22] J. L. M. van Mechelen, D. van der Marel, C. Grimaldi, A. B. Kuzmenko, N. P. Armitage, N. Reyren, H. Hagemann, and I. I. Mazin, *Phys. Rev. Lett.* **100**, 226403 (2008); J. T. Devreese, S. N. Klimin, J. L. M. van Mechelen, and D. van der Marel, *Phys. Rev. B* **81**, 125119 (2010).
- [23] S. N. Klimin, J. Tempere, J. T. Devreese, and D. van der Marel, *Phys. Rev. B* **89**, 184514 (2014).
- [24] J. M. Edge, Y. Kedem, U. Aschauer, N. A. Spaldin, and A. V. Balatsky, *Phys. Rev. Lett.* **115**, 247002 (2015).
- [25] M. Ahrens, R. Merkle, B. Rahmati, and J. Maier, *Physica B* **393**, 239 (2007).
- [26] R. M. Fernandes, J. T. Haraldsen, P. Wölfle, and A. V. Balatsky, *Phys. Rev. B* **87**, 014510 (2013).
- [27] D. Valentini, D. van der Marel, and C. Berthod, *Phys. Rev. B* **94**, 024511 (2016).
- [28] In fact, the contribution of the heavy band is dominant: if the interaction is switched off in the light band the calculated  $T_c$  changes by less than a percent, while if the interaction in the heavy band is reduced by 20%,  $T_c$  does not exceed 80 mK at all densities.
- [29] N. Reyren, S. Gariglio, A. D. Caviglia, D. Jaccard, T. Schneider, and J.-M. Triscone, *Appl. Phys. Lett.* **94**, 112506 (2009).
- [30] The samples of Ref. 18 were prepared by pulsed laser deposition [38]. For the transport measurements in a dilution cryostat, field effect devices were realized using the STO substrate as gate dielectric and Hall bars were photolithographically defined. For each magnetic field,  $T_c$  was defined at the midpoint of the transition: in this way the critical fields display a linear temperature behavior for the perpendicular orientation, while in parallel orientation there is a square root temperature dependence. This confirms the 2D nature of the superconducting state across the whole phase diagram. The angular dependence of the critical field allows to determine the coherence length and the effective thickness of the superconducting 2DEL. The in-plane coherence length remains larger than the superconducting thickness for all the dopings [9, 39], which is consistent with the 2D character of the superconducting 2DEL.
- [31] M. Ben Shalom, A. Ron, A. Palevski, and Y. Dagan, *Phys. Rev. Lett.* **105**, 206401 (2010).
- [32] A. Fête, S. Gariglio, C. Berthod, D. Li, D. Stornaiuolo, M. Gabay, and J.-M. Triscone, *New J. Phys.* **16**, 112002 (2014).
- [33] M. Stengel, *Phys. Rev. Lett.* **106**, 136803 (2011).
- [34] M. Basletic, J. L. Maurice, C. Carretero, G. Herranz, O. Copie, M. Bibes, E. Jacquet, K. Bouzehouane, S. Fusil, and A. Barthélemy, *Nat. Mater.* **7**, 621 (2008).
- [35] C. Cancellieri, M. L. Reinle-Schmitt, M. Kobayashi, V. N. Strocov, P. R. Willmott, D. Fontaine, P. Ghosez, A. Filippetti, P. Delugas, and V. Fiorentini, *Phys. Rev. B* **89**, 121412 (2014).
- [36] H.-M. Christen, J. Mannhart, E. J. Williams, and C. Gerber, *Phys. Rev. B* **49**, 12095 (1994).
- [37] C. Richter, H. Boschker, W. Dietsche, E. Fillis-Tsirakis, R. Jany, F. Loder, L. F. Kourkoutis, D. a. Muller, J. R. Kirtley, C. W. Schneider, and J. Mannhart, *Nature* **502**, 528 (2013).
- [38] C. Cancellieri, R. Reyren, S. Gariglio, A. D. Caviglia, A. Fête, and J.-M. Triscone, *Europhys. Lett.* **91**, 17004 (2010).
- [39] S. Gariglio, M. Gabay, J. Mannhart, and J.-M. Triscone, *Physica C* **514**, 189 (2015).